1988MNRAS.235..403T

Mon. Not. R. astr. Soc. (1988) **235,** 403–423

Very extended ionized gas in radio galaxies – IV. PKS 2152−69

C. N. Tadhunter★, R. A. E. Fosbury★ and S. di Serego Alighieri★ *Space Telescope – European Coordinating Facility, European Southern Observatory, Karl-Schwarzschild-Strasse-2, D-8046, Garching bei München, FRG*

J. Bland *Institute for Astronomy, University of Hawaii, Honolulu, Hawaii 96822, USA*

I. J. Danziger *European Southern Observatory, Karl-Schwarzschild-Strasse-2, D-8046, Garching bei München, FRG*

W. M. Goss *National Radio Astronomy Observatory†, PO Box 0, Socorro, New Mexico 87801, USA*

W. B. McAdam *School of Physics, University of Sydney, Sydney, NSW 2006, Australia*

M. A. J. Snijders *Royal Greenwich Observatory, Herstmonceux Castle, Hailsham, East Sussex, BN27 1RP*

Accepted 1988 April 8. Received 1988 April 8; in original form 1988 January 13

Summary. Optical, radio and ultraviolet observations of the luminous southern radio elliptical galaxy PKS 2152−69 are presented. Narrow-band images and long-slit spectra reveal a system of low-ionization filaments extending out to a maximum radius of 20 arcsec (16 kpc; H_0=50 km s^{-1} Mpc^{-1} as used throughout this paper). To the north-east, however, a luminous cloud is found at a distance of 10 arcsec (8 kpc) from the nucleus. This emits lines of extremely high ionization, including [Ne v]λ3426, He II λ4686, [Ca v]λ5309, [Fe VII]λλ6087, 5721 and [Fe x]λ6374. In addition to the lines, the cloud has a continuum that is considerably bluer than that from the underlying stellar population. We find strong ionization gradients within the cloud, with the highest ionization states associated with both the peak in the local blue continuum and the side of the cloud facing the nucleus. The radial ionization gradient indicates that the nucleus is providing the ionizing energy for the cloud, while the tangential ionization gradient and proximity of the cloud to the radio axis suggest that this energy is directed towards it in

★Affiliated to the Astrophysics Division, Space Science Department, European Space Agency.
†Operated by Associated Universities, Inc. under contract with the National Science Foundation.

Downloaded from https://academic.oup.com/mnras/article/235/2/403/982228 by U.S. Department of Justice user on 17 August 2022

© Royal Astronomical Society • Provided by the NASA Astrophysics Data System

1988MNRAS.235..403T

an intense radiation or plasma beam. The jet/cloud interaction hypothesis is further supported by the kinematical evidence for entrainment in the form of faint wings extending 3 000 km s^{-1} to the blue of the [O III] line cores.

1 Introduction

Recent long-slit spectroscopy and narrow-band imaging have revealed systems of emission line gas extending out to tens of kpc from the nuclei of a significant proportion of quasars (Stockton & MacKenty 1987) and radio galaxies with strong nuclear emission lines (Tadhunter 1986). The earlier papers in this series have illustrated the diversity of structures associated with these extended emission line regions (EELR). They range from the rapidly rotating disc in PKS 2158−380 (Fosbury *et al.* 1982: Paper I), to be extended arms with central bar in PKS 0349−27 (Danziger *et al.* 1984: Paper II), to the irregular system of blobs and filaments along the radio axis of PKS 0634−20 (Fosbury *et al.* 1984: Paper III). It is possible that the diversity of forms and kinematics reflects a variety of origins for the extended gas. While the morphological and kinematical evidence support a merger in PKS 2158−380, the relationship between PKS 0349−27 and its neighbours suggests tidal interactions among a small group of galaxies. In other systems in which the EELR have an irregular structure (e.g. NGC 1275: Kent & Sargent 1979; M87: Ford & Butcher 1979) the gas may have originated internally by cooling from the hot (10^{6-8} K) phase of the galactic or intergalactic medium (e.g. Fabian, Nulsen & Canizares 1984). Whatever its exact origin, the gas will eventually relax through dissipation and fall into stable orbits in the galaxy potential. This process of relaxation will inevitably lead to an exchange of angular momentum and a net infall of warm gas into the nucleus, perhaps fuelling the AGN.

Thus the EELR can provide information about the origins of both the gas and the activity but they are also important in other respects. As systems of well-defined blobs and filaments at known projected distance from the nuclei, they act as excellent laboratories for testing our ideas about physical processes in active galaxies in general. Their overall emission line spectra are well modelled in terms of photoionization by a continuum with a significant EUV component. However, it has been difficult to explain their large emission line luminosities in terms of photoionization by an isotropic power-law continuum from the nucleus (Papers I and II; Tadhunter 1986). This has stimulated further modelling which has shown that the emission line ratios and luminosities of the EELR are better explained if the nuclear continuum has the form of a hot ($T\sim1$–2×10^5 K) thermal spectrum (Robinson *et al.* 1987).

Photoionization by the nucleus is not the only possibility, however. In some systems the EELR are clearly interacting with extended radio structures (van Bruegel *et al.* 1985: hereafter VB85). Although the physics of such interactions is not yet well understood, it is clear that they are a two-way process: the radio jet can ionize, compress and accelerate the ISM, but, at the same time, the jet can be distorted and deflected by the interaction (VB85). Thus we can also gain an understanding of radio jets and their ionizing role by studying the EELR.

The radio source PKS 2152−69 was first identified with a galaxy by Westerlund & Smith (1966). Some of the basic properties of the galaxy are listed in Table 1. Its general optical appearance on survey plates, absolute magnitude and *B–V* colour are all consistent with it being a giant E or D galaxy, although it has a bluer *U–B* colour than expected for such galaxies and coadded scans by the *IRAS* satellite reveal an infrared excess at 25 and 60 μm (Golombek, Miley & Neugebauer 1987). Both of these latter properties may be related to the activity in the nucleus or, alternatively, enhanced star formation in parts of the galaxy.

The total radio power of PKS 2152−69 places it in the realm of the powerful radio sources, well above the break in the radio luminosity function (e.g. Auriemma *et al.* 1977). The early radio maps (Schwarz, Cole & Morris 1973; Schilizzi & McAdam 1975) showed a steep-spectrum

Downloaded from https://academic.oup.com/mnras/article/235/2/403/982228 by U.S. Department of Justice user on 17 August 2022

© Royal Astronomical Society • Provided by the NASA Astrophysics Data System

1988MNRAS.235..403T

Table 1. The basic properties of PKS 2152−69. References: a: Westerlund & Wall (1969) 39 arcsec aperture; b: Westerlund & Smith (1966); c: this paper; d: Price & Milne (1965); e: galactic reddening from Burstein & Heiles (1982); f: Golombek *et al.* (1987).

Optical and Infrared			**Radio**		
z	0.0282	c			
B	14.78	a	S_{5GHz}	13.4 *Jy*	d
$B-V$	0.99	a	$\alpha(F_\nu \propto \nu^{+\alpha})$	−0.7	d
$U-B$	0.21	a			
E_{B-V}	<0.03	e			
$S_{60\mu m}$	0.27 *Jy*	f			
Morphology	E3	b	Morphology	Double	c
Major Axis PA	135 ± 5°	c	Radio Axis PA	23 ± 3°	c
M_b	−21.4		P^{tot}_{5GHz}	5×10^{25} *W Hz*$^{-1}$	
$P_{60\mu m}$	9×10^{23} *W Hz*$^{-1}$				

($F_\nu \propto \nu^{-0.7}$) source centred on the galaxy and a flatter-spectrum ($F_\nu \propto \nu^{-0.45}$) source some 3.8 arcmin to the east. The latter was unresolved on the 1.4-GHz Fleurs Synthesis Telescope (FST) map presented by Christiansen *et al.* (1977), and is unlikely to be associated with the main elliptical galaxy. The same FST map resolves the steeper-spectrum source into an elongated structure aligned along PA 14±8°, but fails to reveal any more detailed structure.

PKS 2152−69 is of particular relevance to the question of local ionization because its EELR cover an unusually large range in ionization. In an earlier paper (Tadhunter *et al.* 1987; hereafter T87) we described observations of a high-ionization cloud at a distance of ~8 kpc to the NE of its nucleus and emphasized the similarity between the cloud and an active nucleus. Here we describe more detailed optical, radio and ultraviolet observations of the galaxy which are used to examine whether the cloud is locally ionized by its interaction with the radio jet.

2 Observations

2.1 OPTICAL SPECTROSCOPY

The long-slit spectra were collected between 1978 August and 1986 August on the ESO 3.6-m and the AAT 3.9-m telescopes. A log of observations is presented in Table 2. All the spectra were

Table 2. Details of spectrophotometric observations. The ESO and AAT observations were taken using the Boller & Chivens and RGO spectrographs respectively. The CCD used for the ESO observations was an RCA back-illuminated type SID 501 chip. All the observations were made with the slit centred on the nucleus, except the PA 315° observations for which the slit was centred 7 arcsec east and 7 arcsec north of the nucleus – on the high-ionization cloud.

Date	Instrument	Wavelength Range (Å)	Spec. Res(Å)/ Spat. pix (″)	Slit-width(″)	PA (deg.)	Exposure (mins)
19/08/78	ESO IPCS	3500–7000	12/1.65	2.0	270	60
13/11/82	AAT IPCS	4300–6200	3/2.4	1.5	46	75
13/11/82	AAT IPCS	4300–6200	3/2.4	1.5	125	60
27/07/84	IUE SWP	1200–1950	6/1.4	10.0	47	272
17/08/84	ESO CCD	4500–7500	13/1.15	2.5	225	100
17/08/85	ESO CCD	4500–7500	13/1.15	2.5	290	40
18/08/85	ESO CCD	4500–7500	13/1.15	2.0	315	60
18/08/85	ESO CCD	4500–7500	13/1.15	4.0	315	54
19/08/86	ESO CCD	4500–7500	13/1.15	2.5	280	60
08/08/86	AAT IPCS	3200–7000	6/2.5	3.5	46	56

Downloaded from https://academic.oup.com/mnras/article/235/2/403/982228 by U.S. Department of Justice user on 17 August 2022

© Royal Astronomical Society • Provided by the NASA Astrophysics Data System

1988MNRAS.235..403T

Table 3. Line ratios and fluxes measured from the long-slit spectra.

λ_o(Å)	Identification	Nucleus	LIC	HIC	Seyfert Type 2	3C 277.3 Knot
1216	Lα(total)	36.4	—	—	—	—
1548	C IV	4.1	—	—	—	—
3426	[Ne V]	0.77	—	1.86	1.2	—
3727	[O II]	4.27	>1.5	3.35	3.2	2.5
3868	[Ne III]	0.92	—	1.05	1.4	0.54
4072	[S II], Hδ	0.79	—	—	0.30	—
4340	Hγ(total)	0.53:	—	0.41	—	0.49
4363	[O III]	0.25:	—	0.20	0.21	<0.23
4686	He II	<0.2	—	0.56	0.29	—
4861	Hβ(narrow)	1.00	1.00	1.00	1.00	1.00
5007	[O III]	8.72	1.10	10.04	10.8	10.4
5199	[N I]	0.51	—	—	0.15	—
5309	[Ca V], [Fe XIV]	—	—	0.06:	—	—
5721	[Fe VII]	—	—	0.13	—	—
5875	He I	0.18:	—	0.06:	—	—
6087	[Fe VII], [Ca V]	—	—	0.15	0.10	—
6300	[O I]	3.23	0.52	0.22	0.57	0.55
6370	[O I], [Fe X]	0.98	—	0.14	0.22	—
6562	Hα(total)	{18.3	2.48	3.36	3.10	4.00
6584	[N II]		2.78	1.30	2.9	0.65
6723	[S II]	3.25	2.63	1.02	1.5	1.55
7135	[A III]	0.33:	—	0.21	—	—
$F(H\beta)/10^{-15}$	($erg\ cm^{-2}\ s^{-1}$)	9.6	0.3	2.33	—	5.6
Aperture	($arcsec^2$)	2.5 × 4.6	2.5 × 4.6	4.0 × 4.6		4.0 × 6.0

The ratios for the nucleus and high-ionization cloud (HIC) are a composite of several spectra covering different wavelength regions (see text), but the Hβ fluxes are from the 1985 CCD observations using the apertures shown. The Lα and C IV λ1548 line ratios for the nucleus have also been normalized to the CCD Hβ flux. The low-ionization component (LIC) ratios are for a region centred 8 arcsec east of the nucleus along PA 280°. Columns 6 and 7 are, respectively, the mean high-ionization spectrum from Ferland & Osterbrock (1986) and the spectrum of the knot in 3C277.3 from VB85.

reduced and analysed on the RGO node of the UK STARLINK network with the spectral reduction package SPICA. They were wavelength calibrated using comparison arc spectra taken before and after each galaxy spectrum, and flux calibrated using observations of Oke (1974) white dwarfs. Full details of the reductions are given in Tadhunter (1986).

Table 3 presents line ratios and fluxes measured from the long-slit spectra. No single spectrum covers the full spectral range with good signal-to-noise ratio. Therefore, the ratios for individual regions are from a composite of several spectra. The mean spectrum for the high-ionization cloud is a composite of the four low-dispersion CCD spectra taken in 1985 August (for He II λ4686 to [Ar III] λ7135), the 1982 November intermediate-dispersion IPCS spectrum (for [O III] λ4363 and Hγ) and the 1986 August low-dispersion IPCS spectrum (for [Ne V] λ3346 to [Ne III] λ3889). The mean spectrum for the nucleus is a composite of four low-dispersion CCD spectra from 1985 August (for Hβ to [Ar III] λ7135), the two IPCS spectra from 1982 (for [O III λ4363 and Hγ) and the two low-dispersion IPCS spectra from 1978 and 1986 (for [Ne V] λ3346 to [S II] λ4072). All the line ratios were placed on the same scale via normalization to [O III] λ5007 which was strong in all

Downloaded from https://academic.oup.com/mnras/article/235/2/403/982228 by U.S. Department of Justice user on 17 August 2022

© Royal Astronomical Society • Provided by the NASA Astrophysics Data System

1988MNRAS.235..403T

the spectra. In the parts of the galaxy (e.g. the nucleus and extended low-ionization components: see Section 3.2) where the emission lines were weak relative to the underlying stellar continuum, a template elliptical galaxy spectrum was scaled and subtracted prior to measurement. From the dispersion of line ratios measured on more than one spectrum, we estimate that the numbers in Table 3 are accurate to better than 25 per cent in most cases. Where the uncertainty is greater, because of blending or the weakness of the line, the measurement has been marked with a colon in Table 3.

2.2 NARROW-BAND IMAGING

To investigate more fully the spatial distribution of the ionized gas we obtained a set of narrow-band images in the light of Hα+[N II] and nearby continuum bands using the $f/8$ focus of the ESO/MPIfA 2.2-m telescope in 1985. Details of the images are given in Table 4. A composite of the August 16 and October 2 continuum and continuum subtracted Hα+[N II] images is shown in Plate 1. The reduction, which consisted of bias subtraction, flat-fielding and registering, was carried out at ESO in Garching using the MIDAS data reduction system. Cosmic rays were removed by interpolating a two-dimensional surface fitted to the surrounding pixels.

Table 4. Narrow-band CCD imaging observations. λ and $\Delta\lambda$ are the respective effective wavelengths and bandwidth (FWHM) of the interference filters used in the observations.

Date	Detector	λ (Å)	$\Delta\lambda$ (Å)	Exposure(s)	Comments
1985 August 14	RCA CCD	6770	80	2 × 1200	Hα+[N II]+Continuum
1985 August 14	RCA CCD	6607	76	2 × 600	Continuum
1985 August 16	RCA CCD	6770	80	1800	Hα+[N II]+Continuum
1985 August 16	RCA CCD	6607	76	1200	Continuum
1985 October 2	RCA CCD	6770	80	2400	Hα+[N II]+Continuum
1985 October 2	RCA CCD	6690	80	1200	Continuum

2.3 ULTRAVIOLET SPECTROSCOPY

In order to complement the long-slit spectra and provide estimates of the UV continuum of the nucleus, PKS 2152−69 was also observed at low resolution with the SWP camera of the *International Ultraviolet Explorer* satellite (*IUE* see Boggess *et al.* 1978) in 1984 July (see Table 2 for details). One-dimensional spectra of the nucleus were re-extracted from line-by-line two-dimensional images using the procedure outlined by Tadhunter, Perez & Fosbury (1986).

2.4 RADIO MAPPING

One further data set we include in this study is a radio map made with the Molonglo Synthesis Telescope (MOST: Mills 1981) at 843 MHz. This is shown in Fig. 1. With an effective beamwidth of 43 arcsec (FWHM) it has a higher resolution than any of the other published maps of PKS 2152−69.

3 Results

3.1 THE GALAXY, ITS RADIO STRUCTURE AND ENVIRONS

The optical structure (Plate 1) and absolute magnitude of PKS 2152−69 are typical of powerful radio galaxies. An examination of SERC J survey plates shows that the galaxy is not in a rich,

Downloaded from https://academic.oup.com/mnras/article/235/2/403/982228 by U.S. Department of Justice user on 17 August 2022

© Royal Astronomical Society • Provided by the NASA Astrophysics Data System

1988MNRAS.235..403T

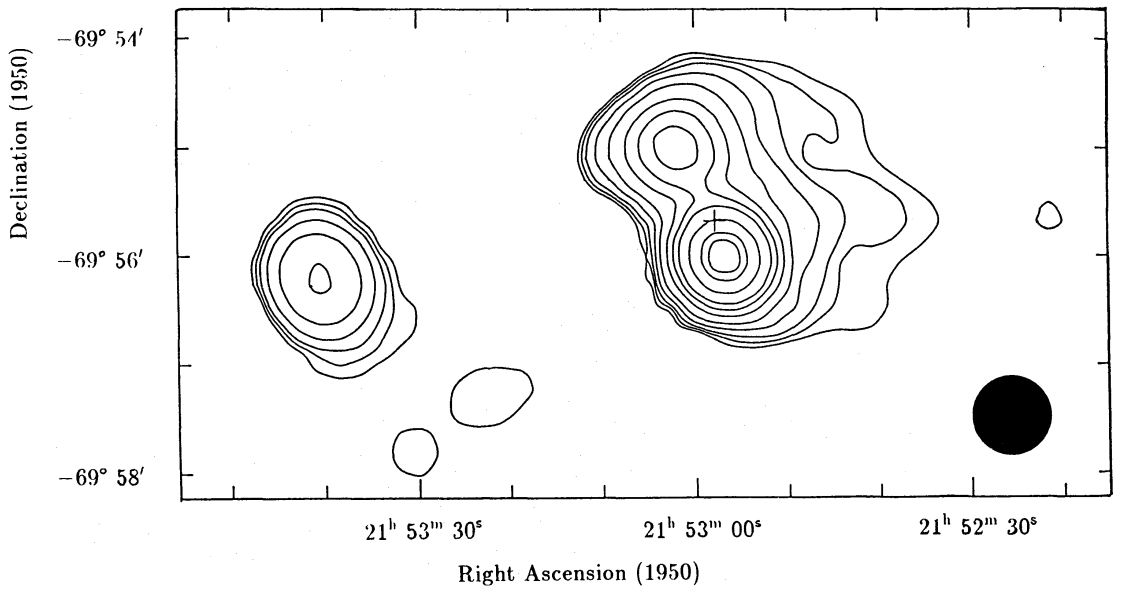

Figure 1. 843-MHz radio map of PKS 2152−69 made with the Molonglo Synthesis Telescope. The beam is indicated by the circle to the lower right of the diagram. The cross marks the position of the elliptical galaxy identified with the radio source. The contour levels are 1.87×(0.075, 0.15, 0.25, 0.5, 1, 2, 3, 4, 6, 8, 9) Jy beam.

centrally condensed cluster environment. Its nearest neighbour is a fainter spiral galaxy at a projected distance of 250 kpc to the north-west. Within a circle of radius 3 Mpc we count less than 50 galaxies, before correction for the field, whereas by the definition of Abell (1958) a rich cluster has more than 50 galaxies within such a radius. Again, this lack of a rich environment is not unusual in powerful radio galaxies (Prestage & Peacock 1988).

Our MOST observation (Fig. 1) resolves the elongated radio structure shown in the map by Christiansen *et al.* (1977) into an unequal double with approximate separation 70±30 kpc. This structure is consistent with classification as an FR II source (Fanaroff & Riley 1974). One interesting feature is the apparent 'trailing' of the lobes to the west: the contours on the eastern side are much steeper on the western side. It is premature to draw detailed conclusions about this structure, but we note that similar distorted 'H' shapes have been observed in galaxies in which strong interactions between the radio jet and the ISM are taking place (Heckman *et al.* 1982; Heckman, van Breugel & Miley 1984).

3.2 THE IONIZED GAS

PKS 2152−69, like many other radio galaxies (Tadhunter 1986), has a complex emission line structure that does not follow the smooth elliptical contours of the underlying stellar component. The continuum-subtracted Hα+[N II] image presented in Plate 1(b) shows an irregular system of blobs, filaments and diffuse structure, in contrast to the regular structures described for PKS 2158−380 and PKS 0349−27 in Papers I and II.

To give a clearer impression of the ionization and distribution of the EELR, the positions in which low- and high-ionization gas was observed along the various slit positions are marked in Fig. 2. 'Low Ionization' in this context is defined to mean any region with a LINER-type spectrum (Heckman 1980), i.e. with [O II]λ3727/[O III]λ5007>1 and [O I]λ6300/[O III]λ5007>0.33. We identify three main emission-line components, which will now be described in turn.

Downloaded from https://academic.oup.com/mnras/article/235/2/403/982228 by U.S. Department of Justice user on 17 August 2022

© Royal Astronomical Society • Provided by the NASA Astrophysics Data System

1988MNRAS.235..403T

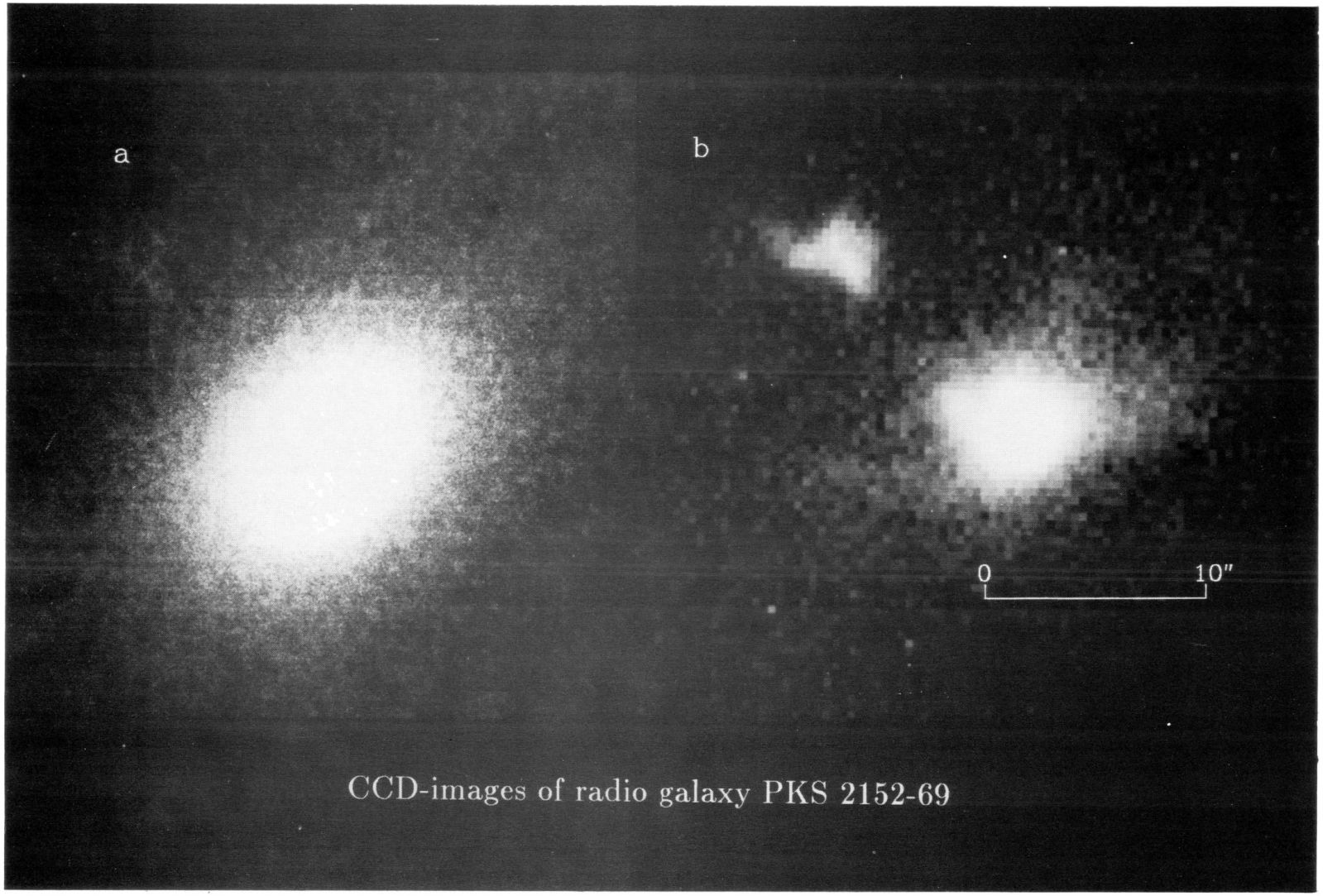

Plate 1. Composite narrow-band CCD images of PKS 2152−69. (a) The continuum image (λ_e=6607 Å; $\Delta\lambda$=76 Å). (b) The continuum subtracted Hα+[N II] image (λ_e=6770 Å; $\Delta\lambda$=80 Å). North is to the top, east to the left.

[facing page 408]

© Royal Astronomical Society • Provided by the NASA Astrophysics Data System

Downloaded from https://academic.oup.com/mnras/article/235/2/403/982228 by U.S. Department of Justice user on 17 August 2022

1988MNRAS.235..403T

Downloaded from https://academic.oup.com/mnras/article/235/2/403/982228 by U.S. Department of Justice user on 17 August 2022

© Royal Astronomical Society • Provided by the NASA Astrophysics Data System

1988MNRAS.235..403T

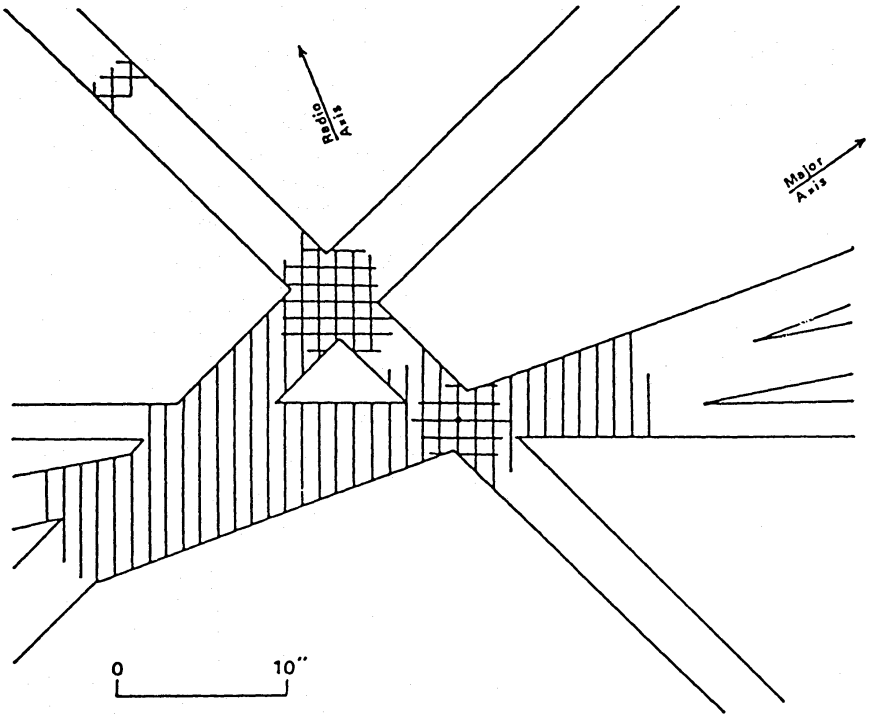

Figure 2. The locations along the various slit positions in which emission lines were observed. Hatched: low-ionization gas. Cross-hatched: high-ionization gas. See text for more details.

3.2.1 The nuclear component

The nuclear component is the region of intense line emission in the inner few kpc of PKS 2152−69. The nuclear spectrum has been described previously by Marenbach & Appenzeller (1982), Whittle (1982) and Danziger & Goss (1983). It shows marked similarities to the nuclear spectrum of the BLRG Pictor A (Danziger, Fosbury & Penston 1977), with an intermediate ionization state and both forbidden and permitted lines showing broad wings (Fig. 3a; Table 3). Like Pictor A, the broad wings are strongest in the lines with the largest critical densities for collisional de-excitation (e.g. [Ne v]λ3426, [O i]λ6300), a feature that can be explained by a combination of strong velocity-dispersion and density gradients across the inner narrow-line region (Pelat, Alloin & Fosbury 1981; Carswell *et al.* 1984; Filippenko 1985).

The broad permitted-line components have a full width at zero intensity of more than 10 000 km s^{-1}. Their strength places PKS 2152−69 in an intermediate position between the BLRG (very strong broad components) and the NLRG (no broad components), whereas the form of the optical continuum is closer to the NLRG: it is dominated by a stellar continuum typical of elliptical galaxies, with strong Ca II, Mg II-*b*, Na I-*D* and TiO absorption features. The equivalent widths of Mg II λ5190 and Na I λ5893 are 3.5±0.4 and 4.2±0.5 Å respectively, which is well within the range measured by Tonry (1980) for a large sample of normal early-type galaxies.

Despite the lack of evidence in the optical for a non-stellar component in the nuclear continuum, a faint continuum is detected from the nucleus on our longest-exposure SWP spectrum. It has a flux of 1.0×10^{-15} erg cm^{-2} s^{-1} Å^{-1} at 1800 Å – the approximate peak in the SWP camera sensitivity. This is at the limit of detectability for *IUE* (Snijders 1983), so we can deduce little about the detailed shape of the continuum in the UV; the above flux is probably only accurate to within a factor of two. The UV continuum emission is not spatially extended, and mostly arises from the inner two pixels of the *IUE* large aperture (the inner 3 arcsec). It is therefore reasonable

Downloaded from https://academic.oup.com/mnras/article/235/2/403/982228 by U.S. Department of Justice user on 17 August 2022

© Royal Astronomical Society • Provided by the NASA Astrophysics Data System

1988MNRAS.235..403T

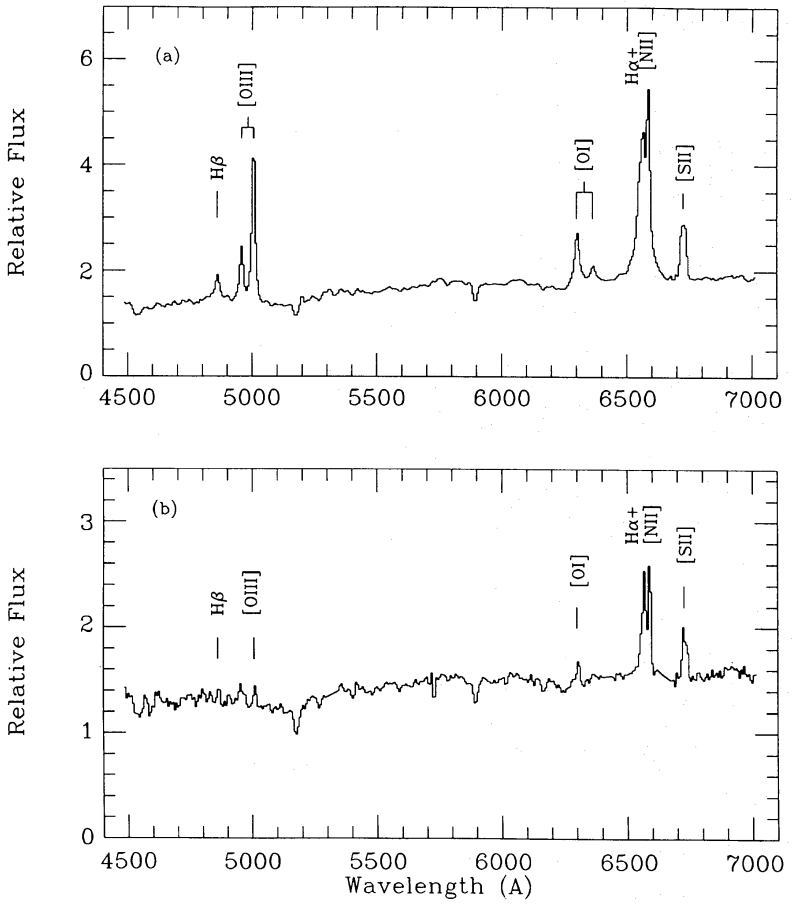

Figure 3. (a) The nuclear spectrum of PKS 2152−69 derived from the 1985 CCD spectra. (b) A sample spectrum of the extended low-ionization component.

to compare the *IUE* continuum fluxes with those from our smaller (2.5×4.6 arcsec^2) aperture optical CCD spectra. We find $F(1800)/F(5000)\sim0.7$ for PKS 2152−69, whereas measurements of normal ellipticals give $F(1800)/F(5000)<0.1$ (e.g. Oke, Bertola & Cappacioli 1980; Burstein *et al.* 1987). Hence there is evidence for a significant continuum excess at UV wavelengths in the nucleus of this galaxy, over and above the expected stellar contribution.

In addition to a faint continuum, we also detect lines of Lα and CIVλ1550 in our SWP spectrum. With a FWHM of 6.8 Å the Lα is only marginally resolved and consists mainly of a narrow component. Comparing the Lα flux to our estimate of the narrow Hβ flux from the CCD spectrum, we find Lα/H$\beta\sim$36. This is likely to be an upper limit for the nuclear narrow-line region as a whole, because the aperture used for the *IUE* observations was much larger than that for the CCD observations. Furthermore, the Lα might be contaminated by broad components that are difficult to detect with the limited resolution of *IUE* at short wavelengths. Thus, although Lα/H$\beta\sim$36 is consistent with the results of detailed photoionization models for zero reddening (e.g. Ferland & Osterbrock 1986), we cannot rule out some intrinsic reddening of the nucleus.

3.2.2 The extended low-ionization component

The extended low-ionization component appears as a system of low-surface-brightness wisps and filaments which cover a large surface area of the galaxy and extend out to a maximum radius of 16 kpc to the east along PA 100° (Plate 1 and Fig. 2). This component shows no clear alignment

Downloaded from https://academic.oup.com/mnras/article/235/2/403/982228 by U.S. Department of Justice user on 17 August 2022

© Royal Astronomical Society • Provided by the NASA Astrophysics Data System

1988MNRAS.235..403T

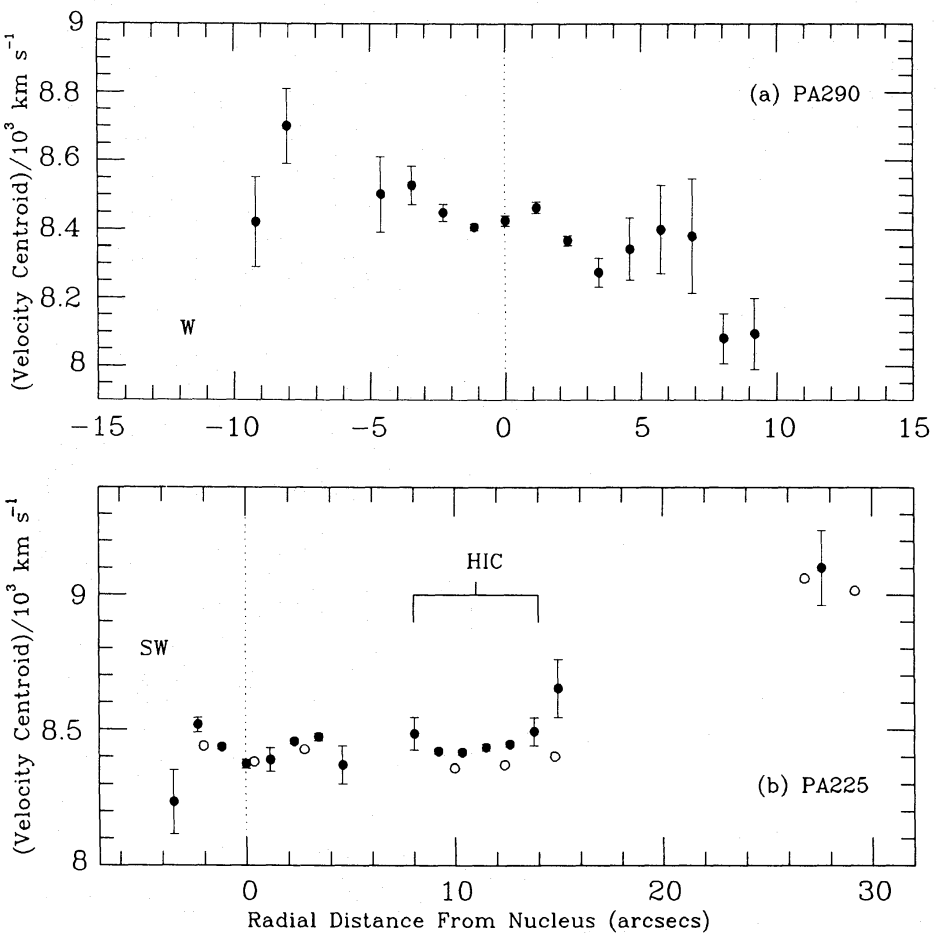

Figure 4. (a) The variation in [O III] λ5007 heliocentric radial velocity along PA 290°. (b) The same as (a) for PA 225°. Closed symbols: 1985 low-dispersion CCD data. Open symbols: 1982 intermediate-dispersion IPCS data. All distances are referred to the centroid of the galaxy continuum along the slit (marked by a dotted line).

with the major or minor axes of the parent elliptical galaxy. A characteristic spectrum is presented in Fig. 3(b) with line ratios listed in Table 3. These show that the ionization state is low, with [O I] λ6300 and Hβ of comparable strength to [O III] λ5007. The continuum properties are similar to those of the nucleus, with strong stellar absorption features and a steep decline in the continuum (in F_λ) at wavelengths shorter than 4300 Å.

In order to investigate the kinematics of this component, the wavelength centroid of the [O III] λ5007 has been measured at several positions along PA 290°. The resulting heliocentric radial velocities are shown in Fig. 4(a), where the vertical bars indicate the estimated error due to noise in both the line and the continuum, calculated according to the prescription of Bohlin *et al.* (1983). In contrast to the results obtained for PKS 2158−380 and PKS 0349−27 in Papers I and II, the velocity field shows no clear pattern, the overall velocity range covered by the bulk of the gas is small (ΔV<400 km s^{-1}) and there is no steep velocity gradient across the nucleus. Similar measurements of the [O II] λ3727 blend along PA 270° produce a velocity field with broadly similar features to those in Fig. 4(a).

3.2.3 The high-ionization cloud

In Plate 1(b) the high-ionization cloud is the bright region 10 arcsec to the north-east of the nucleus. It has a fan-shape and is aligned to within 10° of the minor axis of the galaxy.

Downloaded from https://academic.oup.com/mnras/article/235/2/403/982228 by U.S. Department of Justice user on 17 August 2022

© Royal Astronomical Society • Provided by the NASA Astrophysics Data System

1988MNRAS.235..403T

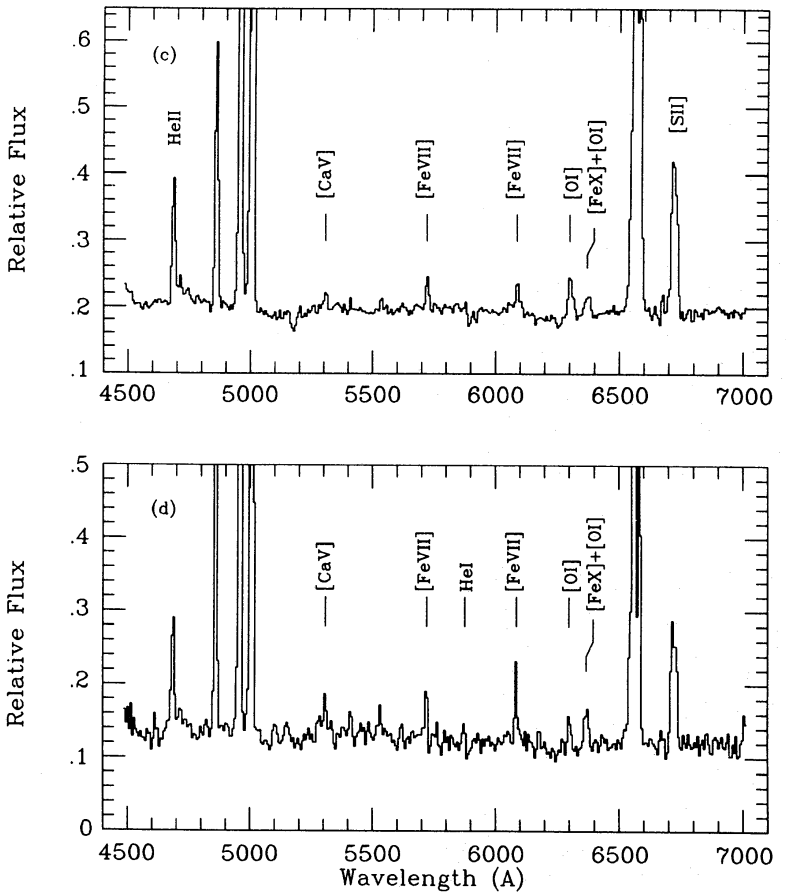

Figure 5. (a) The integrated CCD spectrum of the high-ionization cloud (mean of three CCD spectra). (b) Single spatial section at the peak of the local HIC continuum (PA 315°, 2 arcsec slit), note the great relative strength of the [Fe x]+[O i] blend.

A composite of the three 1985 CCD spectra of this component is shown in Fig. 5(a), with line ratios listed in Table 3. Its spectrum is strikingly different from those of the nucleus and the low-ionization component. Relative to Hβ, the cloud has stronger [Ne v] λ3426, He II λ4686 and [O III] λ5007, and weaker [O I] λ6300 and [N II] λ6584. It also has a large emission-line luminosity, with about a quarter the nuclear Hβ (narrow) luminosity and a much larger surface brightness than any of the other off-nuclear emission-line regions.

The high-ionization state of the cloud is confirmed by the detection of a number of faint diagnostic lines commonly associated with the highest ionization active nuclei (e.g. NGC 1320: de Robertis & Osterbrock 1986). As Fig. 5(a) and (b) shows, these include [Fe VII] $\lambda\lambda$5721, 6087 and [Fe x] λ6374. We also measure a feature at 5308±6 Å, which could be [Ca v] λ5309 or [Fe XIV] λ5303, or a combination of both. Assuming that it is entirely [Ca v] λ5309 we estimate that the [Ca v] λ6087 line, which has an upper level in the same term as [Ca v] λ5309, contributes less than 10 per cent to the feature at λ6087.

Significantly, the highest ionization lines are not present in all parts of the high ionization cloud; they are not as extended as, for example, [O i] λ6300 or [O III] λ5007. The [Fe x] λ6374 is particularly localized. Its presence in the composite spectrum (Fig. 5a) is only indicated by a shift in the centroid of the [Fe x] λ6374+[O i] λ6363 blend by 8 Å to the red of the expected wavelength of [O i] λ6363, and also by the strength of the blend relative to [O i] λ6300. In the spectrum of the highest ionization part of the cloud (Fig. 5b), however, the [Fe x] λ6374 is at least as strong as [O i] λ6300.

Downloaded from https://academic.oup.com/mnras/article/235/2/403/982228 by U.S. Department of Justice user on 17 August 2022

© Royal Astronomical Society • Provided by the NASA Astrophysics Data System

1988MNRAS.235..403T

While the overall spectrum of the cloud shows great similarities to spectra from high-ionization Seyfert 2 nuclei, there are notable differences. Column 6 of Table 3 shows the average spectrum for high-ionization Seyfert 2 galaxies from Ferland & Osterbrock (1986). Compared to this, the high-ionization cloud has much stronger He II λ4686 and weaker [O I] λ6300. The modelling presented in T87 shows that these extreme features can still be made consistent with photoionization models if the cloud consists of a combination of matter- and radiation-bounded components (see also Section 4.4).

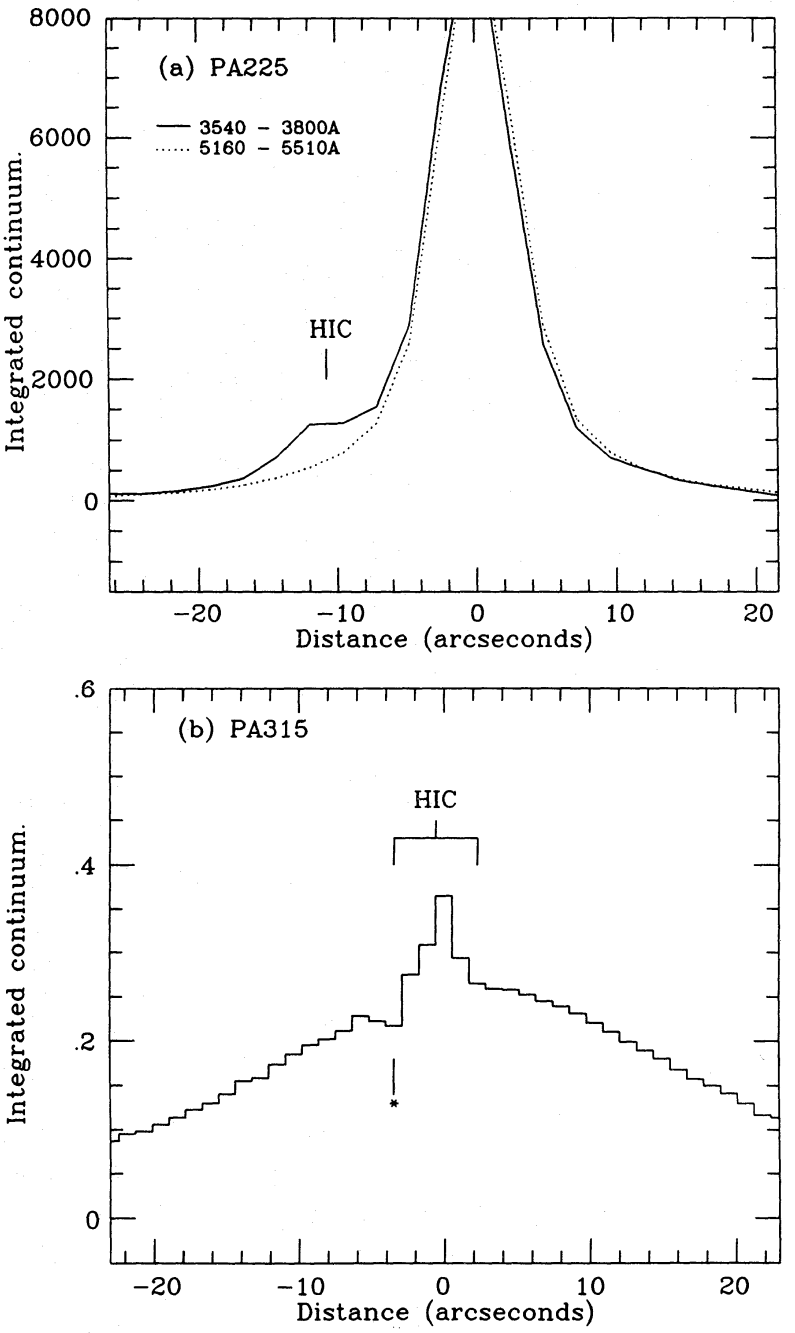

Figure 6. (a) The integrated continuum distribution along PA 225° for two different wavelength ranges. Both distributions have been normalized to the peak flux along the slit. HIC marks the position of the high-ionization cloud. The pixel coordinates are relative to the centroid of galaxy continuum along the slit. (b) The integrated continuum distribution through the high-ionization cloud along PA 315°. The asterisk marks the position of a bad column on the CCD. The pixel coordinates are relative to the peak in the local continuum within the cloud.

Downloaded from https://academic.oup.com/mnras/article/235/2/403/982228 by U.S. Department of Justice user on 17 August 2022

© Royal Astronomical Society • Provided by the NASA Astrophysics Data System

1988MNRAS.235..403T

Apart from the emission-line ratios, a further important difference between the cloud and the other two components is that it has a much bluer continuum. This is best seen in Fig. 6a, which shows the distribution of continuum along PA 225° (slit through both cloud and nucleus) for two different wavelength ranges, each chosen to avoid bright emission lines. The hump associated with the cloud is much stronger relative to the nucleus in the shorter wavelength continuum window (3450–3700 Å). The relative blueness of the continuum can also be seen by comparing Fig. 5(a) and (b) with Fig. 3(a) and (b).

The PA 315° tangential slit position (through the cloud, but not the nucleus) gives better discrimination between the continua of the cloud and the galaxy. From Fig. 6(b) it is clear that there is a sharp peak in the continuum at the site of the cloud, superimposed on the shallower continuum bump from the underlying galaxy. The difference between the centroids of the continuum and [O III] λ5007 distributions along the slit is only 0.1 ± 0.1 arcsec, thus demonstrating a close relationship between the ionized gas and continuum within the cloud in this direction. Because of the difficulty of correcting for the galaxy component along PA 225°, the distribution of the local continuum is less clear in that direction, although we note that the continuum and emission line peaks appear to be displaced, with the continuum peaking on the side of the cloud facing the nucleus. After correction for the underlying galaxy component, we estimate that the blue continuum has a flux of $2\pm0.5\times10^{-17}$ erg cm^{-2} s^{-1} Å^{-1} at 5000 Å.

Despite the differences in ionization and continuum, we cannot distinguish the cloud kinematically from the low-ionization component on the basis of line centroid measurements. Fig. 4(b) shows the radial velocity field measured from the [O III] λ5007 line along PA 46°. Out to a radius of at least 12 kpc there is no strong velocity gradient; we can limit the radial velocity difference between the nucleus and the cloud to $\Delta V<100$ km s^{-1}. Note that the vertical shift between the IPCS and CCD measurements is consistent with the expected systematic error in the wavelength scale.

Fig. 4(b) does, none the less, show one interesting feature of the velocity field along PA 46°. This is a high-velocity component detected in [O III] $\lambda\lambda$5007, 4959 at a distance of 25 kpc to the

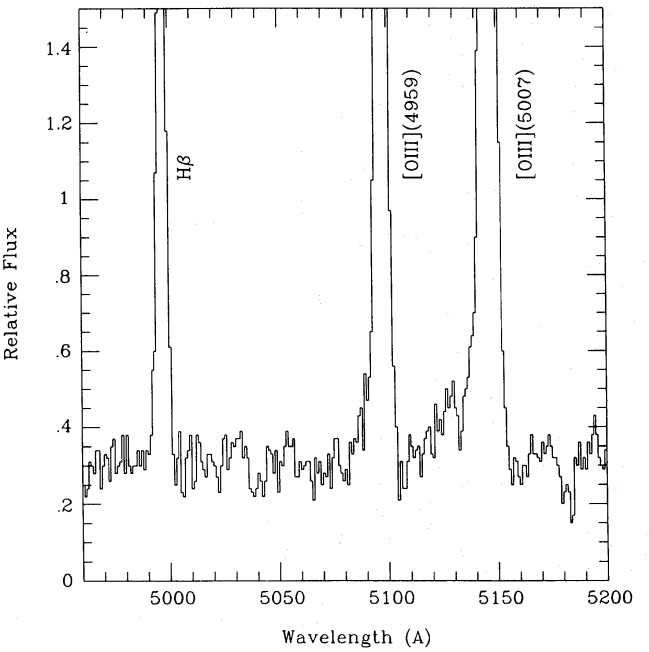

Figure 7. An enlarged plot of the 1982 intermediate-dispersion IPCS (PA 46°) spectrum showing the broad blue-asymmetric wings at the bases of the [O III] lines.

Downloaded from https://academic.oup.com/mnras/article/235/2/403/982228 by U.S. Department of Justice user on 17 August 2022

© Royal Astronomical Society • Provided by the NASA Astrophysics Data System

1988MNRAS.235..403T

north-east of the nucleus on both the IPCS and CCD spectra. It has a radial velocity difference of $+650\pm50$ km s^{-1} with respect to the nucleus. It is not detected in Hα+[N II], so its ionization state appears closer to the high-ionization cloud than the low-ionization component. The relationship of this high-velocity cloud to the other components of ionized gas in the galaxy is uncertain, but it cannot be gravitationally bound to the main elliptical galaxy.

One final noteworthy feature of the cloud is its emission line profiles. Fig. 7 presents an enlarged plot of our intermediate-dispersion IPCS spectrum. This shows broad wings extending up to 3000 km s^{-1} to the short-wavelength side of cores of the [O III] λ5007, 4959 lines. The cores themselves have a width of 160 ± 50 km s^{-1} after quadratic correction for the instrumental profile. The wings are too faint to distort the overall velocity field measured from the emission line centroids (Fig. 4) and only a small fraction of the [O III] emitting region is involved in the strongly blueshifted motions.

4 Discussion

4.1 THE ORIGIN OF THE IONIZED GAS

The structures and velocity fields in PKS 2158−380 and PKS 0349−27 (Papers I and II) led to the conclusion that the ionized gas was accreted, either as a result of mergers or tidal interactions. We have seen that PKS 2152−69 is different in several respects from these latter galaxies: the structure and kinematics of the EELR show no definite pattern, and the overall velocity amplitude (excluding the high-velocity component) and velocity gradient across the nucleus are significantly smaller. Projection effects might mask larger velocity gradients and it will take time following an accretion event for the gas to settle into a regular kinematical and morphological pattern, so we cannot exclude that the gas in PKS 2152−69 has been accreted from an external source. Nevertheless, the gross differences between PKS 2152−69 and the other two galaxies lead us to consider other possibilities.

A plausible alternative to accretion is suggested by the great similarities between the EELR in PKS 2152−69 and the systems of filaments surrounding galaxies near the centres of rich clusters such as NGC 1275 (Kent & Sargent 1979) and M87 (Ford & Butcher 1979). The latter also have irregular velocity fields and structures. Furthermore, their spectra are generally of low ionization, similar to the extended low-ionization component in PKS 2152−69. It has often been suggested (e.g. Fabian *et al.* 1984) that these filaments are formed by cooling from the hot gaseous haloes that surround the central galaxies. Indeed, the kinematics and structure of the filaments are just what one would expect from such a cooling process: the thermal instabilities that lead to the formation of the filaments are expected to produce an irregular distribution of EELR, not necessarily following the contours of the underlying galaxy. If the hot haloes are the result of accumulated stellar mass-loss, then they and the filaments cooling from them will have low specific angular momenta like the stars themselves. PKS 2152−69 has not yet been observed at X-ray wavelengths, but the results of Forman, Jones & Tucker (1985) show that it is luminous enough to have a substantial hot halo. An internal 'cooling flow' is therefore a plausible origin for the warm emission-line gas we observe in this galaxy.

4.2 WHAT IONIZES THE HIGH-IONIZATION CLOUD?

We have shown that the high-ionization cloud has many properties that are not shared by the other components of gas in the same galaxy. Perhaps the most striking of these is the extreme high-ionization state. How then, is the cloud ionized?

One possibility is photoionization by the active nucleus. To test this we start by assuming that

Downloaded from https://academic.oup.com/mnras/article/235/2/403/982228 by U.S. Department of Justice user on 17 August 2022

© Royal Astronomical Society • Provided by the NASA Astrophysics Data System

1988MNRAS.235..403T

the ionizing continuum from the nucleus is isotropic and has a power-law ($F_\nu \propto \nu^{+\alpha}$) shape. By equating the number of ionizing photons entering the cloud with the number of recombinations to hydrogen, it then can be shown that the predicted Hβ flux ($F^{p}_{H\beta}$) from the cloud is related to the measured continuum flux (F^{m}_{λ}) at wavelength λ by

$$F^{p}_{H\beta} = \frac{19.54\, C_f}{-\alpha} \left(\frac{\lambda}{\lambda_0}\right)^{2+\alpha} F^{m}_{\lambda} \text{ erg cm}^{-2} \text{ s}^{-1} \quad (1)$$

where C_f is the fraction of the continuum source covered by the cloud, λ_0 is the wavelength of the Lyman limit and Case B recombination has been assumed. This relation is relatively insensitive to temperature, but in deriving it we have assumed an electron temperature of 17 000 K, which is consistent with the measured [O III] (5007+4959)/4363 line ratio in the low-density limit.

If the nucleus 'sees' the same area of cloud as we do, then we estimate $C_f < 0.01$. Substituting this into the equation along with our estimate of the continuum flux at 1800 Å, the values of $F^{p}_{H\beta}$ shown in the second column of Table 5 are obtained. Comparing these with the actual Hβ flux measured from our widest-slit CCD spectra ($F^{0}_{H\beta}$) we see that the Hβ fluxes are much smaller than observed. In other words, if the continuum is a power-law and radiated isotropically, the nucleus cannot photoionize the cloud.

Table 5. Predicted Hβ fluxes for the high-ionization cloud, calculated according to equation (1).

	Photoionization by Nucleus		Local Photoionization	
α	$F^{p}_{H\beta}/10^{-15}$	$F^{o}_{H\beta}/F^{p}_{H\beta}$	$F^{p}_{H\beta}/10^{-15}$	$F^{o}_{H\beta}/F^{p}_{H\beta}$
−0.5	1.1	2.1	10	0.23
−1.0	0.38	6.0	2.1	0.92
−1.5	0.18	12	0.61	3.8
−2.0	0.10	24	0.20	12.0
	erg cm^{-2} s^{-1}		erg cm^{-2} s^{-1}	

Similar results were obtained for the EELR around PKS 2158−380 and PKS 0349−27 in Papers I and II. A way around the problem is to invoke an ionizing continuum with a hot blackbody shape, or some other shape that peaks in the EUV but has little flux at UV or optical wavelengths. Such a continuum actually produces as good a fit to the overall emission line spectra (Robinson *et al.* 1987), but it still does not explain why the high-ionization cloud has a much higher ionization state and larger emission-line surface brightness than the EELR in all other directions.

We are then left with two possibilities: photoionization by anisotropic radiation field from the nucleus, with the intense component directed towards the cloud, or local ionization. Several strands of evidence suggest that the radiation fields from AGN might be beamed, including the existence of superluminal jets, the statistics of core-dominated radio sources and the rapid variations in BL Lac objects. Recently, Unger *et al.* (1987) have shown that the emission lines in some Seyfert galaxies are much more extended along the radio axis than in other directions – just as expected if the ionizing continuum has been beamed in that direction.

The idea of an anisotropic radiation field should also be taken seriously in the case of PKS 2152–69, because the high-ionization cloud is close to the radio axis (see next section). On the other hand, the presence of an unusually blue continuum within the cloud can argue in favour of local ionization. It is important to consider whether the local continuum is powerful enough to photoionize the cloud. Substituting the estimated local continuum flux at 5000 Å into equation (1) along with $C_f = 1$, we obtain the estimates of $F^{p}_{H\beta}$ shown in the fourth column of Table 5. Comparing these estimates with the measured Hβ flux we see that the local continuum can

Downloaded from https://academic.oup.com/mnras/article/235/2/403/982228 by U.S. Department of Justice user on 17 August 2022

© Royal Astronomical Society • Provided by the NASA Astrophysics Data System

1988MNRAS.235..403T

Table 6. Ionization gradients within the high-ionization cloud: PA 315°, 4 arcsec slit. The spatial coordinates are referred to the section in which the local blue continuum has its maximum intensity.

	Pixel Coordinate (*arcsec*)			
Ratio	−2.3	−1.15	0.00	1.15
He II λ4686/Hβ	0.19	0.40	0.46	0.33
[O III] λ5007/Hβ	7.14	8.94	10.20	11.92
[Fe VII] λ6087/Hα	—	0.05	0.05	—
[O I] λ6300/Hα	0.11	0.06	0.04	0.04:
[N II] λ6584/Hα	0.75	0.50	0.28	0.50
[S II] λ6725/Hα	0.50	0.41	0.21	0.30
$F(H\beta/10^{-16})$ $erg\ cm^{-2}\ s^{-1}$	2.85	8.33	9.32	3.13

photoionize the cloud, but only if the covering factor is high and the ionizing spectrum flat. A large covering factor is reasonable in this case because the continuum source appears to be embedded in the cloud. Moreover, some of the continuum flux may have been missed by the slit. Therefore, it is plausible that the local continuum photoionizes the cloud.

Further clues to the ionization of the cloud are obtained by examining the spatial gradients in the line ratios. Table 6 and Fig. 8(a) show the variations of some important line ratios along the tangential slit direction (PA 315°). Clearly, large ionization gradients are present. The high-ionization lines (e.g. He II λ4686, [Fe VII] λλ 6087, 5721) are strongest relative to the low-ionization lines (e.g. [O I] λ6300, [N II] λ6584, [S II] λ6725) in the central two spatial sections (at −1.15 and 0.00 in Table 8). In fact, [Fe VII] λλ6087, 5721 are only detected in these sections, while [O I] λ6300, a line of similar maximum strength to [Fe VII] λ6087, is far more extended. Of particular importance is the fact that the high-ionization lines are relatively strongest in the section in which the local continuum has its maximum intensity (see Fig. 8a).

[Fe X] λ6374 is also associated with the local continuum. Although its line flux gradients are not obvious from our wide-slit observations along PA 315° because of contamination from a low-ionization region in which [O I] is strong, our narrower-slit observations along the same PA show that it is also strongest in the section of maximum intensity for the local continuum. As can be seen from Fig. 5(b), in this section the [Fe X] λ6374+[OI] λ6363 blend is stronger than [OI] λ6300.

Thus there is a strong association between ionization state, line flux (see also last section) and the local blue continuum within the cloud. This result is consistent with either the local ionization or the anisotropic radiation field pictures. In the former, the blue continuum represents the optical continuation of an ionizing continuum generated *in situ*. In the latter, the continuum is not generated locally but is scattered from the radiation beam into the line-of-sight by material in the cloud. The strong tangential ionization gradients then imply that the bulk of the ionizing radiation is beamed into a cone with opening angle less than 10°.

4.3 THE ORIGIN OF THE LOCAL IONIZING ENERGY

If we accept that the high-ionization cloud is locally ionized, how is the local ionizing energy generated? Again, the ionization gradients provide a clue. Fig. 8(b) and Table 7 show the ionization gradients along a radial slit position (PA 225°) passing through both the cloud and the nucleus. In this direction the ionization state decreases from the side of the cloud facing the nucleus, to the side of the cloud furthest from the nucleus. The blue continuum also peaks on the nucleus side of the cloud.

This indicates that the ionization of the cloud is connected with the nucleus. A plausible source

Downloaded from https://academic.oup.com/mnras/article/235/2/403/982228 by U.S. Department of Justice user on 17 August 2022

© Royal Astronomical Society • Provided by the NASA Astrophysics Data System

1988MNRAS.235..403T

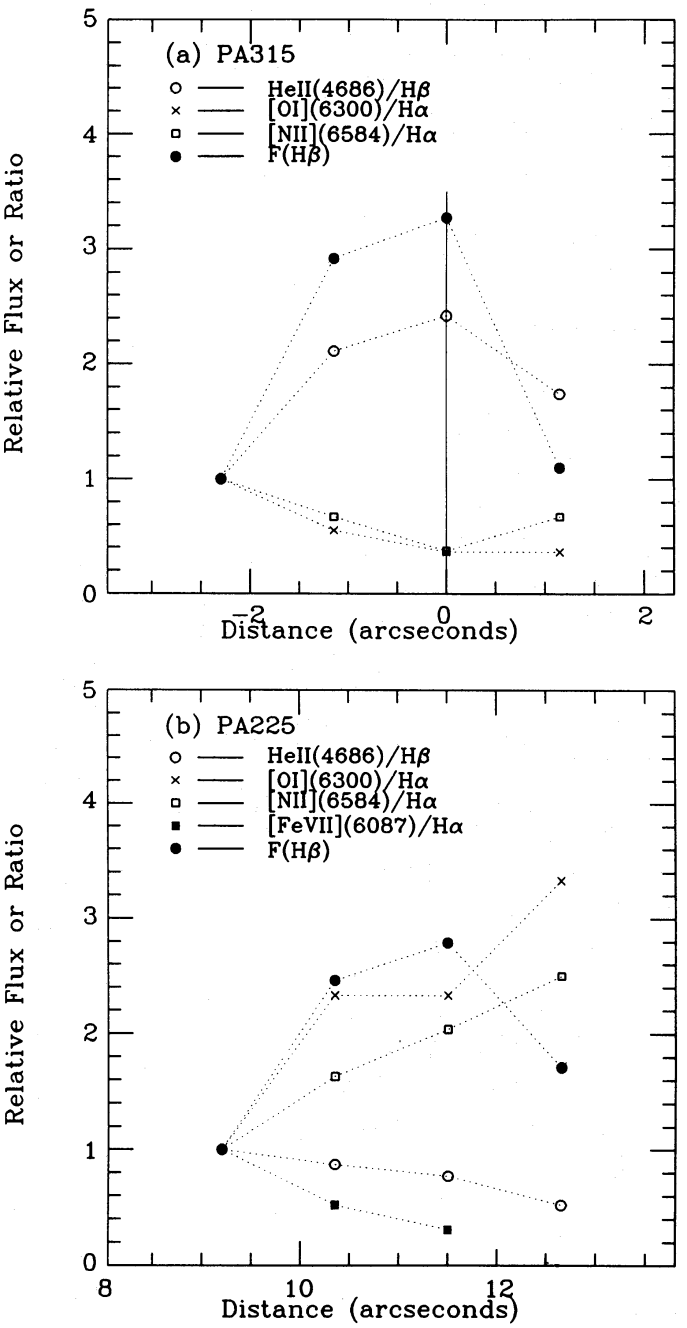

Figure 8. (a) Ionization gradients through the high-ionization cloud along PA 315°. The line ratios and fluxes have been normalized to section with spatial coordinate −2.3 arcsec. The coordinates are referred to the section in which the local continuum peaks (marked by a vertical line). (b) Ionization gradients through the cloud along PA 225°. The line ratios have been normalized to the section at 9.20 arcsec to the north-east of the nucleus. The coordinates are referred to the centroid of the galaxy continuum emission along the slit.

of local ionizing energy, that is also associated with the nucleus, is the plasma jet responsible for carrying energy to the outer radio lobes. Unfortunately, our MOST map (Fig. 1) is of too low resolution to resolve any radio jet and allow us to look directly for a jet/cloud interaction. We can, however, look for an association between the radio axis and the axis through the nucleus and the cloud. The radio axis joining the two lobes resolved in the MOST map is in PA 23±2°, while the cloud/nucleus axis covers PAs 35–50°. Thus, the offset between the two axes is only 12–25°.

Downloaded from https://academic.oup.com/mnras/article/235/2/403/982228 by U.S. Department of Justice user on 17 August 2022

© Royal Astronomical Society • Provided by the NASA Astrophysics Data System

1988MNRAS.235..403T

Table 7. Ionization gradients within the high-ionization cloud: PA 225°, 2.5 arcsec slit. The pixel coordinates are referred to the centroid of the galaxy continuum along the slit.

	Pixel Coordinate (*arcsec*)			
Ratio	9.20	10.35	11.50	12.65
He IIλ4686/Hβ	0.71	0.62	0.55	0.37
[O III]λ5007/Hβ	6.98	8.62	9.80	9.24
[Fe VII]λ6087/Hα	0.08	0.04	0.02	—
[O I]λ6300/Hα	0.03	0.07	0.07	0.10
[N II]λ6584/Hα	0.22	0.36	0.45	0.55
[S II]λ6725/Hα	0.11:	1.06	1.34	1.18
$\hat{F}(H\beta/10^{-16})$ *erg cm*$^{-2}$ *s*$^{-1}$	2.4	5.9	6.7	4.1

Given the low resolution of the map and the apparent distortion of the radio structure, this is small enough to be consistent with the idea of a jet/cloud interaction.

A jet/cloud interaction is also supported by the resemblance between the cloud and the high-ionization knot in 3C277.3 (VB85), which is known from high-resolution radio mapping and narrow-band CCD images to be interacting with the radio jet. The points of similarity include:

(i) The forms of the emission line spectra. The last column of Table 3 gives the emission line ratios for the knot in 3C277.3. In comparison with the high-ionization cloud it has similar [O III]λ5007/Hβ, [O II]λ3727/[O III]λ5007 and [N II]λ6584/Hα ratios. It is not yet clear whether the knot in 3C277.3 has strong He IIλ4686, [Fe VII]$\lambda\lambda$6087, 5721 and [Fe X]λ6374, because the VB85 observations are of insufficient signal-to-noise ratio to show such weak features.

(ii) The presence of a local optical continuum with sufficient strength, on extrapolation to the EUV, to photoionize the gas in the clouds. Both the knot in 3C277.3 and the cloud in PKS 2152−69 have such continua, which are rare in the EELR as a whole (Tadhunter 1986). The optical continuum in 3C277.3 is associated with a radio hotspot for which Miley *et al.* (1981) have measured a radio to optical spectral index of $\alpha\sim-0.7$.

(iii) The offset between the cloud/nucleus axis and the radio axis defined by the outer radio lobes. This is 12–25° for PKS 2152−69 and 10–15° for 3C277.3. Such offsets may be related to bending and deflection of the radio jets by interaction with the emission line clouds.

One way in which PKS 2152−69 differs from 3C277.3 is that there is no large radial velocity difference between the high-ionization cloud and the nucleus. Fig. 4 shows that the motions of the cloud in PKS 2152−69 fit in with general motions of the (low-ionization) gas in the galaxy. In contrast, the large velocity gradient between the high ionization knot and the nucleus in 3C277.3 has been taken as evidence for entrainment of ISM in the radio jet of that galaxy (VB85). This difference between the two objects is not necessarily against the idea of a jet/cloud interaction in PKS 2152−69 for two reasons. First, a larger velocity difference between the cloud and the nucleus might be masked by projection effects. Second, there is *some* evidence for entrainment in the high-ionization cloud, in the form of the blue asymmetric wings to the [O III] lines (Fig. 7). It is indeed difficult to think of a mechanism other than entrainment that could produce these asymmetric profiles in an isolated cloud. The differences in the overall velocity fields might arise because the amounts of material interacting with the radio plasma are different in each case. In PKS 2152−69 the faintness of the broad wings suggests that only a small part of the cloud is currently entrained. Note that if the broad wings are indicating entrainment, the large radial velocity difference of the high-velocity component discovered along PA 46° is unlikely to be also

Downloaded from https://academic.oup.com/mnras/article/235/2/403/982228 by U.S. Department of Justice user on 17 August 2022

© Royal Astronomical Society • Provided by the NASA Astrophysics Data System

1988MNRAS.235..403T

due to entrainment, because the high-velocity component is redshifted, while the broad wings are blueshifted.

Other examples of optical emission associated with extended radio structures have a synchrotron spectrum characterized by a steep-spectrum power law at long wavelengths and a cut-off in the optical or UV (Meisenheimer & Röser 1986). If the high-ionization cloud in PKS 2152−69 is photoionized, the emission-line spectra place stringent constraints on the frequency of any cut-off (ν_c) in the local blue continuum. From the strength of He II λ4686, the continuum must be relatively strong below the He^+ ionization edge. Therefore, ν_c must be greater than 1.3×10^{16} Hz – much higher than for the other cases of jets and lobes in which ν_c has been measured directly (Meisenheimer & Röser 1985; Keel 1986).

A jet/cloud interaction appears to us the most plausible explanation, but there are other ways of explaining the local ionization of the cloud. One possibility we cannot rule out with the present data is that the cloud represents a companion galaxy with its own active nucleus. None the less, there are several pieces of evidence against this. These include the association of the cloud with the radio axis, the association between nucleus and the ionization gradients in the cloud and the presence of highly ionized gas with unusual kinematic properties (see Section 3.2) at much larger radii along the same PA. Furthermore, if the cloud is a companion galaxy that only appears close to the parent nucleus because of projection effects, then we must explain the presence of an active nucleus in a dwarf galaxy with an irregular appearance. Véron-Cetty & Véron (1986) have shown that, among the H I rich galaxies, the type of emission-line activity we observe in the cloud is most common in early-type spirals. It is a rare among late-type spirals and almost unknown in the irregular galaxies. Most difficult to rule out is the possibility that the cloud represents the stripped nucleus of a galaxy merging with the main elliptical. However, as discussed above, the structure and kinematics of the ionized gas in PKS 2152−69 are not similar to other cases in which mergers appear to be taking place.

None of these pieces of evidence against the cloud as separate active nucleus is individually strong, but together they add up to make the possibility seem unlikely. The real test of the jet/cloud interaction hypothesis will come with higher resolution radio observations. If it is correct, these should show – as in all other well-established jet/cloud interactions – a radio hotspot near the cloud and signs of a radio jet leading to that hotspot from the nucleus.

4.4 IONIZATION MECHANISMS WITHIN THE HIGH-IONIZATION CLOUD

The diagnostic diagram presented in Robinson *et al* (1987) show that most of the line ratios in the integrated spectrum of the cloud are consistent with photoionization by a continuum with a significant EUV component. In detail, the best fits are obtained by modelling the cloud as a combination of matter- and radiation-bounded components (T87), with much of the high-ionization line emission (e.g. He II λ4686) emitted by the matter-bounded component, and much of the low-ionization line emission (e.g. [O I] λ6300) emitted by the radiation-bounded component. By changing the relative proportions of the two components across the cloud it is also possible to reproduce the ionization gradients (Robinson & Binette, private communication 1987).

Despite the general success of the photoionization models, they fail to explain the strength of some features in the spectrum. Perhaps the most serious failure is the [O III] λ4363 line which is a factor of four too weak, indicating a much lower electron temperature in the model than measured from the [O III] (5007+4959)/4363 diagnostic in the cloud assuming the low-density limit. Another major problem is [Fe X] λ6374. Penston *et al.* (1984) have claimed that the general correlations observed between the strengths of this and lower-ionization lines in AGN suggest that it is formed by photoionization, but the strength of [Fe X] λ6374 predicted by the otherwise successful models for high-ionization Seyfert 2 galaxies by Ferland & Osterbrock (1986) is a factor

Downloaded from https://academic.oup.com/mnras/article/235/2/403/982228 by U.S. Department of Justice user on 17 August 2022

© Royal Astronomical Society • Provided by the NASA Astrophysics Data System

1988MNRAS.235..403T

of 20 smaller than observed. Although the high-ionization cloud is in some ways an extreme case, the failure to explain the strength of these weak lines is a general problem for high-ionization AGN and EELR. It may indicate that mechanisms other than pure photoionization are at work.

One alternative mechanism that may be relevant in the context of jet/cloud interactions is ionization by cosmic rays from the plasma beam. The preliminary models by Ferland & Mushotsky (1984), involving a combination of both cosmic-ray and photo-ionization, show that one of the primary effects of the cosmic rays is to heat the gas and produce higher electron temperatures. This mechanism is therefore particularly attractive for the high-ionization cloud with its strong [O III]λ4363 line. The models for cosmic ray ionization are not well developed, however, and the flux of relativistic particles is difficult to estimate in this case, so the exact relevance of cosmic ray ionization to the cloud is uncertain.

Another plausible mechanism is collisional ionization in a hot shocked region. Shocks might be expected wherever the radio plasma interacts with the ISM. Pedlar *et al.* (1985) have suggested, for example, that hot shocks form around radio plasmons expanding into the warm ISM. Provided the temperature in the shock is high enough $-\sim 10^6$ K for optimum formation of [Fe x] lines for a gas in collisional equilibrium – and the amount of material in the shock large enough, we should observe significant coronal line emission from the shock. If this mechanism applies to the formation of [Fe x]λ6374 in the cloud, then the formation of the local ionizing continuum might also be associated with the shock, since the regions of emission of the blue continuum and [Fe x]λ6374 appear to be spatially coincident. The identification of [Fe x] with the region of formation of the continuum is also attractive for AGN in general, because it may help explain the correlations between [Fe x] and the lower ionization lines formed by photoionization.

Overall, a full model of the structure and ionization of the high-ionization cloud is likely to be highly complex, with a number of mechanisms operative.

5 Conclusions

This study of PKS 2152−69 has illustrated the variety of phenomena associated with activity in radio galaxies. The variety is manifest in the kinematics and structure of the EELR – the chaotic kinematics and structure and generally low velocity amplitudes are consistent with an internal cooling flow origin for most of the gas, but we also observe an extended high-velocity component moving at more than 600 km s^{-1} with respect to the nucleus, and evidence in the line profiles for large-scale motions within an isolated cloud. The variety is even clearer in the ionization states of the EELR which cover the full range seen in the general population of AGN: from LINER to high-ionization Seyfert 2. It is significant that the extremes – both in terms of ionization and kinematics – are associated with a particular direction, possibly related to the extended radio structure. This and the other evidence presented above lead us to conclude that energy is being directed from the nucleus to the high-ionization cloud in a narrow beam, either of radiation, or of relativistic plasma. In the latter case, the cloud represents a spectacular example of the type of jet/ISM interaction seen in some other galaxies (e.g. van Breugel 1985, and references therein).

Future high-resolution studies of PKS 2152−69 using the Australia Telescope in the radio and the Hubble Space Telescope in the optical/UV will answer questions about the way energy is transported from the nucleus to the cloud. In addition, such studies will provide new insights to some of the long-standing problems in AGN research, to which we have shown this object is relevant.

Acknowledgments

We are grateful to the European Southern Observatory for support in the form of generous allocations of observing time. The paper is based in part on observations with the *International*

Downloaded from https://academic.oup.com/mnras/article/235/2/403/982228 by U.S. Department of Justice user on 17 August 2022

© Royal Astronomical Society • Provided by the NASA Astrophysics Data System

1988MNRAS.235..403T

Ultraviolet Explorer obtained at the European Space Agency's Villafranca Satellite Tracking Station. We are also grateful to the PATT for valuable observing time, and to the Anglo–Australian Observatory for the 1986 service observation. We thank Andrew Robinson and Luc Binette for freely discussing the results of the model calculations. CT acknowledges financial support in the form of an SERC studentship. This work was completed while CT held an ESA fellowship.

References

Abel, G., 1958. *Astrophys. J. Suppl.,* **3,** 211.
Auriemma, C., Perola, G. C., Ekers, R., Fanti, R., Lari, C., Jaffe, W. J. & Ulrich, M-H., 1977. *Astr. Astrophys.,* **57,** 41.
Boggess, A. *et al.,* 1978. *Nature,* **275,** 382.
Bohlin, R. C., Hill, J. K., Jenkins, E. B., Savage, B. D., Snow, T. P., Spitzer, L. & York, A. G., 1983. *Astrophys. J. Suppl.,* **51,** 277.
Burstein, D. & Heiles, C., 1982. *Astr. J.,* **87,** 1165.
Burstein, D., Bertola, F., Buson, L. M., Faber, S. M. & Lauer, T. R., 1987. Preprint.
Carswell, R. F., Baldwin, J. A., Atwood, B. & Phillips, M. M., 1984. *Mon. Not. R. astr. Soc.,* **286,** 464.
Christiansen, W. N., Frater, R. H., Watkinson, A., O'Sullivan, J. D., Lockhart, I. A. & Goss, W. M., 1977. *Mon. Not. R. astr. Soc.,* **181,** 183.
Danziger, I. J. & Goss, W. M., 1983. *Mon. Not. R. astr. Soc.,* **202,** 703.
Danziger, I. J., Fosbury, R. A. E., Goss, W. M., Bland, J. & Boksenberg, A., 1984. *Mon. Not. R. astr. Soc.,* **208,** 589 (Paper II).
Danziger, I. J., Fosbury, R. A. E. & Penston, M. V., 1977. *Mon. Not. R. astr. Soc.,* **179,** 41P.
de Robertis, M. M. & Osterbrock, D. E., 1986. *Astrophys. J.,* **301,** 98.
Fabian, A. C., Nulsen, P. E. J. & Canizares, C. R., 1984. *Nature,* **316,** 733.
Fanaroff, B. L. & Riley, J. M., 1974. *Mon. Not. R. astr. Soc.,* **167,** 31P.
Ferland, G. J. & Mushotzky, R. F., 1984. *Astrophys. J.,* **286,** 42.
Ferland, G. J. & Osterbrock, D. E., 1986. *Astrophys. J.,* **300,** 658.
Filippenko, A. V., 1985. *Astrophys. J.,* **289,** 475.
Ford, H. C. & Butcher, H., 1979. *Astrophys. J. Suppl.,* **41,** 147.
Forman, W., Jones, C. & Tucker, W., 1985. *Astrophys. J.,* **293,** 102.
Fosbury, R. A. E., Boksenberg, A., Snijders, M. A. J., Danziger, I. J., Disney, M. J., Goss, W. M., Penston, M. V., Wamsteker, W., Wellington, K. J. & Wilson, A. S., 1982. *Mon. Not. R. astr. Soc.,* **201,** 991 (Paper I).
Fosbury, R. A. E., Tadhunter, C. N., Bland, J. & Danziger, I. J., 1984. *Mon. Not. R. astr. Soc.,* **208,** 955 (Paper III).
Golombek, D., Miley, G. K. & Neugebauer, G., 1988. *Astr. J.,* **95,** 26.
Heckman, T. M., 1980. *Astr. Astrophys.,* **87,** 152.
Heckman, T. M., Miley, G. K., Balick, B., van Breugel, W. J. M. & Butcher, H. R., 1982. *Astrophys. J.,* **299,** 41.
Heckman, T. M., van Breugel, W. J. M. & Miley, G. K., 1984. *Astrophys. J.,* **286,** 509.
Keel, W. C., 1986. *Astrophys. J.,* **302,** 296.
Kent, S. M. & Sargent, W. L. W., 1979. *Astrophys. J.,* **230,** 667.
Marenbach, G. & Appenzeller, I., 1982. *Astr. Astrophys.,* **108,** 95.
Meisenheimer, K. & Röser, H.-J., 1986. *Nature,* **319,** 459.
Miley, G. K., Heckman, T. M., Butcher, H. R. & van Breugel, W. J. M., 1981. *Astrophys. J.,* **247,** L5.
Mills, B. Y., 1981. *Proc. astr. Soc. Aust.,* **4,** 156.
Oke, J. B., 1974. *Astrophys. J. Suppl.,* **27,** 21.
Oke, J. B., Betola, F. & Capaccioli, M., 1980. *Astrophys. J.,* **243,** 453.
Pedlar, A., Unger, S. W., Dyson, J. E. & Meaburn, J., 1985. In: *Cosmical Gas Dynamics,* p. 65, ed. Kahn, F. D., VNU Science Press, Utrecht, The Netherlands.
Pelat, D., Alloin, D. & Fosbury, R. A. E., 1981. *Mon. Not. R. astr. Soc.,* **195,** 787.
Penston, M. V., Fosbury, R. A. E., Boksenberg, A., Ward, M. J. & Wilson, A. S., 1984. *Mon. Not. R. astr. Soc.,* **208,** 347.
Prestage, R. M. & Peacock, J. A., 1988. *Mon. Not. R. astr. Soc.,* **230,** 131.
Price, R. M. & Milne, D. K., 1965. *Aust. J. Phys.,* **18,** 329.
Robinson, A., Binette, L., Fosbury, R. A. E. & Tadhunter, C. N., 1987. *Mon. Not. R. astr. Soc.,* **227,** 97.
Schilizzi, R. T. & McAdam, W. B., 1975. *Mem. R. astr. Soc.,* **79,** 1.
Schwarz, U. J., Cole, D. J. & Morris, D., 1973. *Aust. J. Phys.,* **26,** 661.

Downloaded from https://academic.oup.com/mnras/article/235/2/403/982228 by U.S. Department of Justice user on 17 August 2022

© Royal Astronomical Society • Provided by the NASA Astrophysics Data System

1988MNRAS.235..403T

Snijders, M. A. J., 1983. *ESA IUE Newsletter,* **16,** 10.
Stockton, A. & MacKenty, J. W., 1987. *Astrophys. J.,* **316,** 584.
Tadhunter, C. N., 1986. *DPhil thesis,* University of Sussex.
Tadhunter, C. N., Fosbury, R. A. E., Binette, L., Danziger, I. J. & Robinson, A., 1987. *Nature,* **316,** 733.
Tadhunter, C. N., Perez, E. & Fosbury, R. A. E., 1986. *Mon. Not. R. astr. Soc.,* **219,** 555.
Tonry, J. L., 1980. *PhD thesis,* Harvard University.
Unger, S. W., Pedlar, A., Axon, D. J., Whittle, M., Meurs, E. J. A. & Ward, M. J., 1987. *Mon. Not. R. astr. Soc.,* **228,** 671.
van Breugel, W. J. W., 1985. *Can. J. Phys.,* **64,** 392.
van Breugel, W., Miley, G., Heckman, T., Butcher, H. & Bridle, A., 1985. *Astrophys. J.,* **290,** 496 (VB85).
Véron-Cetty, M. P. & Véron, P., 1986. *Astr. Astrophys. Suppl.,* **66,** 335.
Westerlund, B. E. & Smith, L. F., 1966. *Aust. J. Phys.,* **19,** 181.
Westerlund, B. E. & Wall, J. V., 1969. *Astr. J.,* **74,** 335.
Whittle, M., 1982. *PhD thesis,* University of Cambridge.

Downloaded from https://academic.oup.com/mnras/article/235/2/403/982228 by U.S. Department of Justice user on 17 August 2022

© Royal Astronomical Society • Provided by the NASA Astrophysics Data System